Eur. Phys. J. B **7**, 263–269 (1999)

THE EUROPEAN PHYSICAL JOURNAL B

EDP Sciences

Quantitative Brewster angle microscopy measurements of chiral symmetry breaking and chiral boundaries in fatty acid Langmuir monolayers

C. Lautz and Th.M. Fischer[a]

Institute of Experimental Physics I, University of Leipzig, 04103 Leipzig, Germany

Received: 26 January 1998 / Revised: 3 August 1998 / Accepted: 7 August 1998

Abstract. Brewster angle microscopy (BAM) measurements of the low temperature region of the phase diagram of eicosanoic acid monolayers at an acidic subphase are performed. The existence of a new chiral I phase intervening between the L_2 and L_2' phase recently discovered by Durbin *et al.* [M.K. Durbin, A. Malik, A.G. Richter, R. Ghastkadvi, T. Gog, P. Dutta, J. Chem. Phys. **106**, 8216 (1997)] using grazing incidence X-ray diffraction (GIXD) is confirmed. Chiral symmetry breaking within the monolayers creates characteristic boundaries separating domains of opposite handedness. These disclination lines are associated with a jump in the tilt azimuth of the director, while the underlying hexatic orientation is continuous across the boundary. The disclination lines are observed with the Brewster angle microscope and analyzed as a function of surface pressure. The jump in tilt azimuth is determined. Agreement with an extended Landau theory proposed by Durbin is achieved.

PACS. 68.10.-m Fluid surfaces and fluid-fluid interfaces

1 Introduction

Spontaneous breaking of parity, *e.g.*, the occurrence of chirality has attracted scientific interest in a variety of completely different systems. In elementary particle physics, neutrinos only occur with a defined handedness. Naturally occurring macromolecules such as DNA or amino acids exclusively are produced as enantiomeres of one specific chirality. The main idea for the explanation of these experimental observations has been spontaneous breaking of chiral symmetry, *e.g.*, as the parameters of an initially non chiral system changes, the non chiral minimum of the free energy of the system splits into two distinct minima of opposite handedness. As a consequence, the realization of the system exhibits a defined chirality.

It is a question of current interest, whether two dimensional systems, such as monolayers at the air/water interface, exhibit similar behavior. Various attempts have been made both theoretically and experimentally to clarify this question. They were discussed in detail by Durbin *et al.* [1] and will be mentioned briefly in this paper. Couplings have been proposed [2,3] between different order parameters (tilt angle, bond orientation, distortion) relevant for monolayer phases of non chiral molecules, where chiral symmetry breaking should occur. Grazing incidence X-ray diffraction (GIXD) studies [3] and optical observation of monolayer textures [4] have confirmed some of these coupling terms.

In the paper of Durbin *et al.* GIXD and pressure area isotherms are used to show the existence of a new chiral phase in eicosanoic acid. The authors associate the phase behavior with a coupling of the chain tilt azimuth with the distorted hexatic bond orientational order. It is found that the first order *swiveling* transition between the low surface pressure L_2 phase with nearest neighbor (NN) tilt and the higher surface pressure L_2' phase with next nearest neighbor (NNN) tilt, splits into two separate transitions with an intervening chiral I phase at intermediate pressures on an acidic subphase. The questions addressed in the current paper are strongly related to the work of Durbin *et al.* The texture of this chiral phase on a mesoscopic scale can be observed using Brewster angle microscopy (BAM). The chiral order parameter, *e.g.*, the tilt azimuth is determined as a function of the surface pressure by measuring the reflectivity of domains of opposite handedness. These domains are separated by chiral disclination lines with a jump in the tilt azimuth. It is demonstrated that these disclination lines naturally occur in the model of Durbin *et al.* if one includes Frank elastic energy terms. A combination of Durbin's model with a model of Selinger and Nelson [2] yields a phase diagram consistent with the experiment.

2 Experimental

The experimental setup used consists of a home-built BAM. A small area of the BAM image is projected onto a

[a] e-mail: `fischert@rz.uni-leipzig.de`

photon counter by a beam splitter *via* a monomode fiber. This allows measurements of intensity in the BAM image of defined regions within the monolayer. The experimental setup is mostly identical to the BAAS [5,6] setup described previously. Only modifications necessary for the requirements of the presented experiments are mentioned here. A 100 μm pin hole in front of the monomode fiber joined to the photon counter restricts the spot of measurement of the monolayer to less than 10 μm in diameter, so that the reflected light intensity of one single domain can be measured. The monolayer is laterally moved with μm precision using a $x-y$-table fixed to the film balance. All measurements were done with simultaneous observation of the BAM image. Due to attenuation of the image on passing through the silvered spot of the beam splitter, one knows that the spot of measurement is located within the darkened region within the BAM image. The exact position of the spot of measurement was marked on the monitor by calibrating with the reflected light from a TEM grid positioned under the microscope. Together with the $x-y$-table the reflected intensity of any spot within the monolayer may be determined with an relative accuracy of 3%. To prevent dust contamination and lateral flow of the monolayer the whole film balance is enclosed within a PMMA box.

Eicosanoic acid (pH = 3.9 measured in chloroform) was obtained from Sigma Aldrich and claimed to be 99+% pure. Without further purification it was spread from chloroform (p.a. Merck) onto the subphase (pH = 2 $\pm$ 0.2) consisting of pure water (Millipore Milli-Q at 18 MΩ cm) and HCl contained in a home-built Teflon$^{\mathrm{TM}}$ trough described in reference [5].

3 Optical visualization of phase transitions

A rich variety of phases and their transitions in Langmuir monolayers have been observed using BAM [7–10]. All of them are associated with characteristic changes within the texture of such phases as the phase boundary between both phases is crossed. A loss of contrast is observed with BAM, when compressing the monolayer from the tilted L_2'', L_2, L_2' or Overbeck (OV) phases towards the untitled CS, S, LS(Rot I) or LS(Rot II) phases. This contrast is approximately proportional to the square of the tilt angle [5] and changes discontinuously for first order transitions. For second order transitions it continuously decays to zero contrast. Other transitions involving a change of packing of the molecules like the occurrence of herring bone ordering (L_2/L_2'' transition) or change of the tilt azimuth with respect to the bond orientational order (L_2/OV transition and L_2/L_2' transition) show characteristic changes of the organization of domains. Movements of domain walls separating neighboring domains of different tilt azimuth associated with significant conversion of large regions of the domains is characteristic of the low temperature L_2/L_2' *swiveling* transition, on the other hand the formation of brighter or darker domains within a previous uniform domain is typical for the L_2/OV transition occurring at higher temperatures.

Measurements carried out in this paper are focused to the phase behavior of eicosanoic acid on an acidic subphase at low (-5 ± 10 °C) temperatures. As mentioned above a new chiral phase with the tilt azimuth pointing into a direction intermediate between NN and NNN has been discovered at an intermediate surface pressure by Durbin *et al.* It intervenes between the low pressure L_2 phase and the high pressure L_2' phase. The L_2/I transition was found to be of first and the I/L_2' transition to be of second order.

4 Results

Typical BAM images (analyzer angle 80°) on expansion of the eicosanoic acid monolayer are shown in Figures 1a–1d at a subphase temperature $T = 1.8$ °C for surface pressures $\pi = 19.1$ mN/m to 13.9 mN/m. The changes in the texture observed when crossing the L_2'/I transition are shown in Figure 1a (L_2' phase, $\pi = 19.1$ mN/m) and Figure 1b (I phase, $\pi = 17.8$ mN/m). Some domains – separated from neighboring domains by permanent and non-chiral boundaries (solid lines in Fig. 1e) – showing a uniform gray value in the L_2' phase split in two domains of slightly different intensity separated by a newly formed disclination wall (dotted lines in Fig. 1e) when expanding in the I phase. This effect is most pronounced for domains appearing bright or dark in the L_2' phase and not resolved for domains of intermediate gray value. On further expansion the contrast between the new domains, *e.g.*, the jump in gray value across the wall continuously increases (Fig. 1c: I phase, $\pi = 16.3$ mN/m) until the first order transition I/L_2 is reached. To clarify the behavior observed the disclination lines separating the domains in the L_2' phase are drawn as solid lines in Figure 1e, dotted lines represent the newly formed disclinations of the I phase. In the L_2 phase (Fig. 1d: $\pi = 13.9$ mN/m) the domains break up into small areas of different gray values. The change in texture at the I/L_2 transition shows the same characteristics as the first order *swiveling* L_2/L_2' transition observed at higher temperatures ($T = 11$ °C). On performing compression-expansion-cycles across the L_2'/I transition, the disclination walls always appear at the same location indicating that although the wall disappeared in the L_2' phase the distinctive preceding mosaic pattern of the I phase is recovered. Such memory effects were previously observed at other Langmuir monolayer phase transitions [11]. They are usually explained due to a locally preserved anisotropy of the hexatic lattice. Here the influence of elastic stress excerted onto the domains from the permanent disclinations may be another reason. Due to the finite lateral resolution of 3 μm and the relative scatter in counting rate of 3% it is not possible to resolve the internal structure of the disclination wall.

Figure 2 shows the low temperature region of the phase diagram of eicosanoic acid on the acidic subphase (pH $\approx$ 2) where the I phase occurs. Phase transitions observed using BAM are depicted as symbols. Triangles indicate the transition from non tilted phases towards the tilted L_2' phase. Circles represent the second order

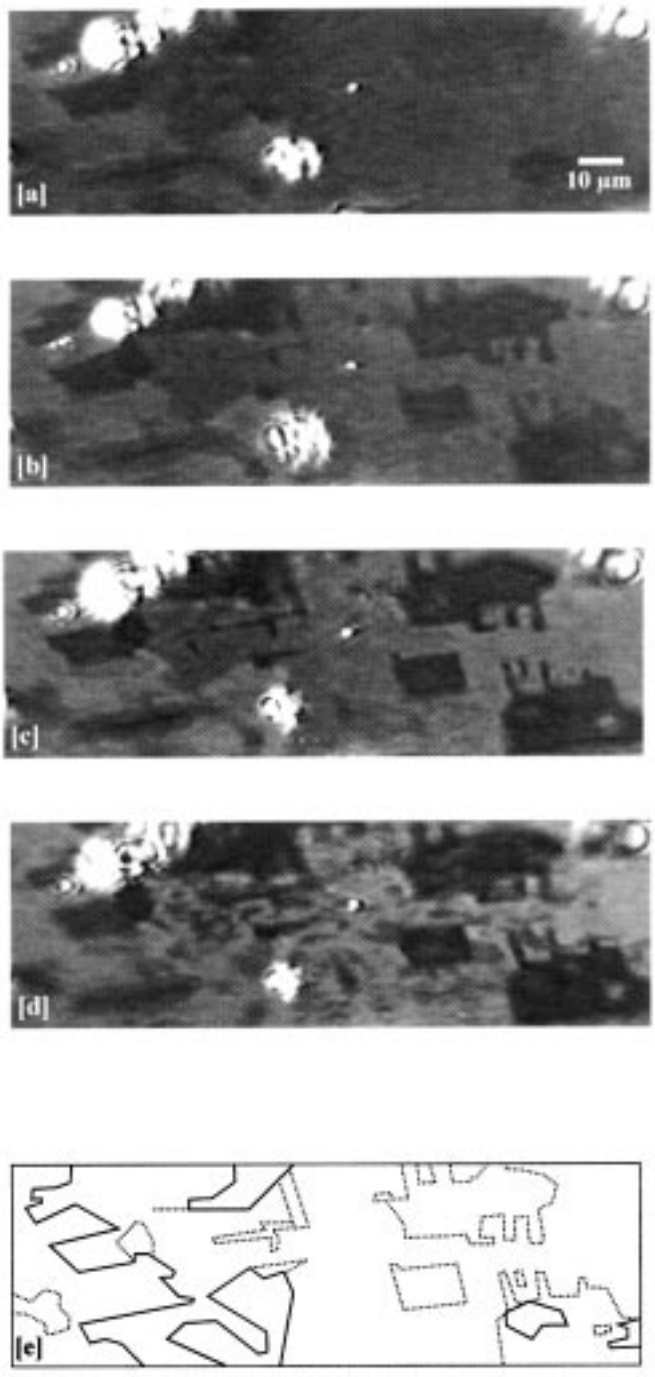

Fig. 1. BAM images of the same area at $T = 1.8$ °C; (a) $\pi = 19.1$ mN/m, (L_2' phase), (b) 17.8 mN/m, (I phase), (c) 16.3 mN/m, (I phase), and (d) 13.9 mN/m, (L_2 phase). (e) Map of the non-chiral disclination lines (solid lines, present in the L_2' and I phase, (a–c) and the chiral disclination lines (dotted lines, present in the I-phase, (b) and (c). The contrast across the chiral disclination lines evolves continuously – indicating a second order transition – from zero to a maximum close to the I/L_2 transition. The first order swiveling I/L_2 transition occurs in a abrupt splitting into smaller domains.

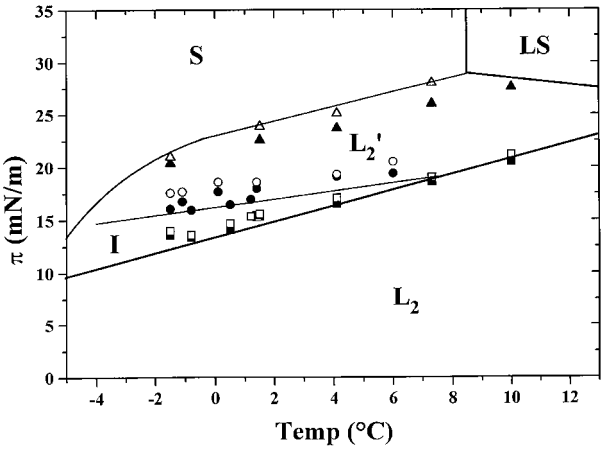

Fig. 2. Low temperature region of the phase diagram of eicosanoic acid on an acidic subphase (pH $\approx$ 2) from BAM measurements. The open dots show results obtained on compression, the solid dots on expansion of the monolayer. Solid lines show phase boundaries obtained from isotherm measurements (from Ref. [1]). Thick lines represent first order, thin lines second order phase transitions.

L_2'/I transition and squares the first order I/L_2 transitions. Open symbols are measured on compression while closed symbols are measured on expansion[1]. Results from isotherm measurements (obtained from Ref. [1]) are added as solid lines to the phase diagram. Good agreement between both data concerning the existence and the position in temperature of the different phase boundaries is achieved, however systematic deviations in pressure of the order of 1–2 mN/m are observed for all transitions. This may be due to slight differences in pH of the subphase. In fact changes of pH (ΔpH ≈ 0.2) lead to shifts of the transition pressure of the order of 1 mN/m. The hystereses observed at a compression expansion cycle is of the order of 2 mN/m.

Durbin *et al.* have shown that the tilt angle within and around the I phase has an approximately constant value of 20°. The same tilt angle is observed for the *swiveling* transition in a variety of systems [12]. For these tilt angles the changes of the reflected intensity from one to another domain is dominated by its dependency on the tilt azimuth of the chains of the molecule. The dependency on the anisotropy of the lattice structure, which is observed in the untitled S phase at high pressure [11] can be neglected. In this case the reflected intensity is described by [13]

$$I_\alpha(\varphi) \propto (A\cos^2\varphi + B + C\sin\varphi + D\sin\varphi\cos\varphi)^2, \quad (1)$$

[1] The differences in transition pressure at the L_2'/I transition on expansion and compression is an artifact due to the difficulty in observation of the low contrast disclinations.

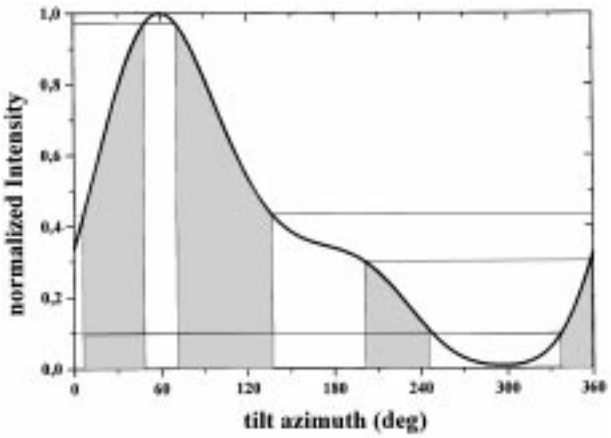

Fig. 3. Normalized reflectivity of a Langmuir monolayer as a function of the tilt azimuth calculated according equation (1) with $\lambda = 514$ nm, $\Theta_B = 53.12°$, $\varepsilon_\perp = 2.31$, $\varepsilon_\perp + \delta\varepsilon = 2.43$, $\vartheta = 20°$, $\alpha = 80°$.

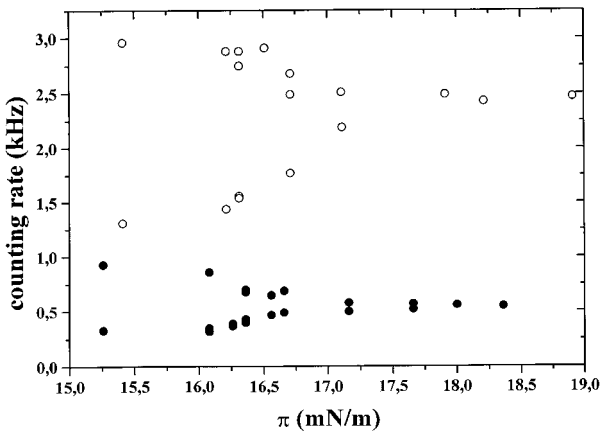

Fig. 4. Reflectivities of domains with higher (○) and lower (●) reflectivities occurring in the L_2' phase and the change of these reflectivities when expanding the monolayer. The counting rates (reflected light intensities) of the photo multiplier used are shown as dots.

where:

$$\begin{cases} A = \dfrac{2\pi d \cos\Theta_B}{\lambda(\varepsilon_\perp + \delta\varepsilon\cos^2\vartheta)} \cos\alpha(\varepsilon_\perp)\delta\varepsilon\sin^2\vartheta \\ B = \dfrac{2\pi d \cos\Theta_B}{\lambda(\varepsilon_\perp + \delta\varepsilon\cos^2\vartheta)} \cos\alpha\Big[(\varepsilon_\perp - 1)(\varepsilon_\perp - \tan^2\Theta_B) \\ \qquad +(\varepsilon_\perp - 1 - \tan^2\Theta_B)\delta\varepsilon\cos^2\vartheta\Big] \\ C = \dfrac{2\pi d \cos\Theta_B}{\lambda(\varepsilon_\perp + \delta\varepsilon\cos^2\vartheta)} 2\sin\alpha\sin\Theta_B\delta\varepsilon\cos\vartheta\sin\vartheta \\ D = \dfrac{2\pi d \cos\Theta_B}{\lambda(\varepsilon_\perp + \delta\varepsilon\cos^2\vartheta)} 2\sin\alpha\cos\Theta_B\varepsilon_\perp\delta\varepsilon\sin^2\vartheta \end{cases} .$$

Here d is the monolayer thickness, $\lambda = 514$ nm the wavelength of the laser, $\Theta_B = 53.12°$ the Brewster angle, $\varepsilon_\perp = 2.31$ and $\varepsilon_\perp + \delta\varepsilon = 2.43$ the dielectric constants perpendicular and along the aliphatic chain [14], $\vartheta = 20°$ the tilt angle, $\alpha = 80°$ the analyzer angle, and φ denotes the tilt azimuth. Equation (1) is plotted as a function of the tilt azimuth in Figure 3 for the values given above and normalized to the maximum intensity which is reached at a tilt azimuth of 60°. It is used to convert counting rates normalized by the maximum counting rate 3.05 kHz (± 0.15 kHz) of the brightest domain found in the monolayer into tilt azimuth values.

Figure 4 shows measurements at $T = 0$ °C of counting rates of a dark respectively bright L_2' domain and the splitting of its counting rate in the I phase measured by moving the corresponding subdomains on either side of the wall under the spot of measurement. This splitting corresponds to a rotation in tilt azimuth to the left respectively to the right, *e.g.*, a broken chiral symmetry. The inversion of equation (1), *e.g.*, the conversion of counting rates to tilt azimuth values is not unique as can be seen in Figure 3. Each counting rate corresponds to two different values of the tilt azimuth. The tilt azimuth as a function of the surface pressure obtained by inversion of equation (1) is plotted as squares for the bright and as circles for the dark domains in Figure 5. Assumed the change of tilt azimuth is the same across all disclination walls independent of the orientation of corresponding subdomains with respect to the laboratory system, it is possible to assign the correct branch of the solution (closed symbols), since only for this situation similar tilt azimuth jumps for both disclination walls are obtained. The jump reaches a value of approximately 50° at $\pi = 15.4$ mN/m close to the I/L_2 transition. At low subphase temperatures the condensation of water drops with high reflectivities ontop of the monolayer occurs as time passes. For this reason the measurements could not be extended to the I/L_2 transition pressure ($\pi = 13.9$ mN/m), however extrapolating the splitting behavior towards the I/L_2 transition pressure gives a final splitting of 60°.

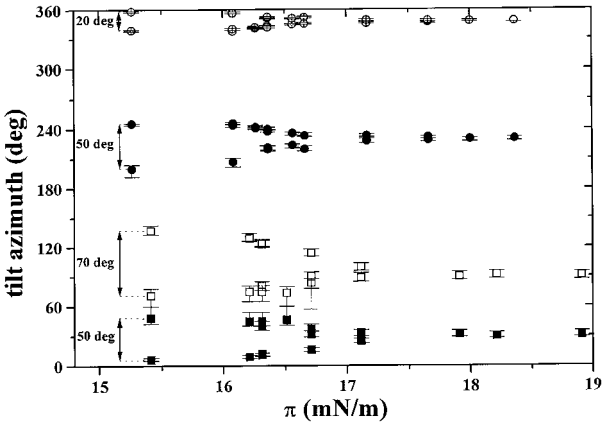

Fig. 5. Absolute tilt azimuth values as a function of the surface pressure calculated from the domain reflectivities shown in Figure 4 using the calibration function (Eq. (1)) in Figure 3. Open and solid symbols correspond to different branches of the inversion of equation (1). The solid symbols correspond to the proper branch (see discussion in the text).

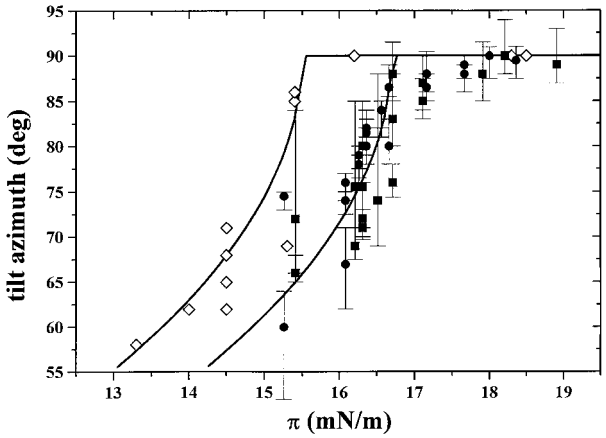

Fig. 6. Changes of the relative tilt azimuth, measured with respect to the non chiral NNN bond, as a function of the surface pressure. (●, ■): BAM, (◇): GIXD (from Ref. [1]). The solid lines are fits according to equation (3).

Durbin *et al.* have shown that the L_2' phase is a NNN phase, *e.g.*, the angle ϕ between the c director and the NN direction along the hexatic deformation axis equals 90°. Assuming that no changes in orientation of the hexatic lattice occurs on compression we may relate the absolute tilt azimuth angle φ measured in the present experiment to the relative tilt azimuth angle ϕ measured by Durbin *et al.* by

$$\phi_I = \frac{\pi}{2} - |\varphi_I - \varphi_{L_2'}|, \tag{2}$$

where the indices refer to the value observed in the two different phases. In Figure 6 ϕ_I is plotted as a function of the surface pressure. The data obtained from BAM counting rate measurements on either side of the disclination walls are shown as closed symbols, squares are from the high reflectivity, circles from the low reflectivity domains. The open diamonds represent the data of Durbin *et al.* obtained from GIXD measurements. Both data are fitted with a mean field behavior

$$\phi_I(\pi) = \phi^0(\pi_c - \pi)^{1/2} \tag{3}$$

where $\phi^0 = 22$ deg $\mathrm{m}^{1/2}\mathrm{mN}^{-1/2}$ and $\pi_c = 16.7$ mN/m for the BAM data and $\pi_c = 15.5$ mN/m [2] for the GIXD data, accounting for the systematic shift in transition pressure observed between both measurements. Apart from this shift both data are consistent with each other. From this agreement one may conclude that the type of disclination wall observed in the Brewster angle microscope is a disclination where the hexatic lattice orientation is unchanged across the wall and it is only the tilt azimuth that changes.

[2] Due to the variation of the subphase pH used for the determination of the phase diagram (Fig. 2) and the counting rate measurements (Figs. 4 and 6) the transition pressures are only consistent with an accuracy of 2 mN/m.

5 Discussion

Durbin *et al.* have proposed a Landau free energy model in which coupling of the lattice distortion with the tilt azimuth competes with coupling of the tilt azimuth with the NNN directions. They could show that according to which of both terms in the Landau free energy dominates all phases L_2, I, and L_2' are predicted by this model. The question addressed in this section is, whether this model does describe the behavior appropriately and whether it is possible to also explain the disclination walls observed in the BAM images. A question of interest is also whether it is possible to understand the merging of the L_2/I and L_2'/I transition lines into a single first order *swiveling* L_2/L_2' transition line at higher temperatures (Fig. 2). There is another Landau free energy proposed by Nelson and Halperin which was used in order to explain the *swiveling* transition [2] and could predict a variety of textures observed for monolayers of simple amphiphiles within the adjacent phases [15]. It also predicts chiral symmetry breaking, but due to different couplings. The Landau energy of Nelson and Halperin contains two order parameters, the bond orientational field $\theta(x)$, describing the direction of NN bonds with respect to a fixed laboratory coordinate system, and the tilt azimuth $\varphi(x)$, measured with respect to the same coordinate system. If there is additionally a distortion in the system a third order parameter field $\Psi(x)$ has to be introduced describing the direction of deformation. In the limit where coupling between the deformation and the bond orientation dominates over the coupling between φ and the two other orientational fields one obtaines

$$F = \frac{1}{2}K_6(\nabla\theta)^2 + \frac{1}{2}K_3(\nabla\varphi)^2 + d_2\cos(2(\theta-\varphi)) - h_6\cos(6(\theta-\varphi)) - h_{12}\cos(12(\theta-\varphi)). \tag{4}$$

The first two terms are elastic energies, the parameter d_2 describes the amount of deformation, h_6 is the hexatic parameter changing its sign at the L_2'/L_2 transition, h_{12} is a next leading contribution to the hexatic order only important if h_6 is small, *e.g.*, near the L_2'/L_2 transition.

With $h_{12} = 0$ (Eq. (4)) describes the free energy proposed by Durbin *et al.*, while for $d_2 = 0$ one regains the free energy of Halperin and Nelson. The equilibrium value of $(\theta - \varphi)$ is given by minimizing F and it only depends on the relative ratio of the three parameters d_2, h_6 and h_{12}. It is therefore convenient to represent the phase diagram on the sphere $d_2^2 + h_6^2 + h_{12}^2 = 1/4$ respectively its stereographic projection from the point d_2, h_6, $h_{12} = 0$, 0, $-1/2$ onto the tangent plane of the sphere in the point d_2, h_6, $h_{12} = 0$, 0, 1/2, *e.g.*, by expressing the parameters in the free energy (4) as

$$d_2 = \frac{d}{1+h^2+d^2},$$
$$h_6 = \frac{h}{1+h^2+d^2},$$
$$h_{12} = \frac{1}{2}\frac{1-h^2-d^2}{1+h^2+d^2}, \tag{5}$$

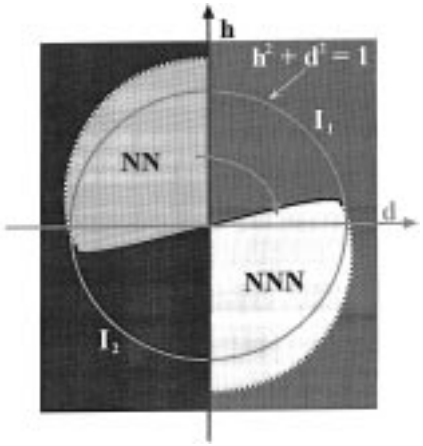

Fig. 7. Phase diagram of the Landau free energy (Eq. (4)) in stereographic projected coordinates (Eq. (7)).

with d and h the coordinates within the tangent plane. In this representation $d_2 = 0$, *e.g.*, the Selinger Nelson model is mapped onto the h axes, while $h_{12} = 0$ the Durbin model is mapped onto the unit circle $h^2 + d^2 = 1$. $h_{12} > 0$ is mapped into the interior, $h_{12} < 0$ into the exterior of the unit circle. Points of constant ratio d_2/h_6 are straight lines $d = (d_2/h_6)h$ through the origin. The phase diagram for the free energy in equation (4) is shown in stereographic projection in Figure 7. It consists of four phases, one NN, one NNN and two chiral intermediate (I_1, I_2) phases. $d_2 = d = 0$, is a first order phase boundary with a jump of 60° in tilt azimuth, separating the NN from the I_1, the NNN from the I_2, and the I_1 from the I_2 phase. A second order boundary line ($h_2 - 9h_6 + 36h_{12} = 0$), *e.g.*, $(d - 1/36)^2 + (h + 1/4)^2 = (1.014)^2$ separates the NNN from the I_1 phase. It starts in the forth quadrant ($d_2 > 0,\ h_6 < 0,\ h_{12} < 0$) outside the unit circle at $(d,\ h) = (0, -1.261)$ moves to the first quadrant ($d_2 > 0,\ h_6 > 0,\ h_{12} < 0$) intersects the unit circle $h_{12} = 0$ and ends within the unit circle ($d_2 > 0,\ h_6 > 0,\ h_{12} > 0$) at the bicritical point $(d,\ h) = (0.98,\ 0.14)$ where the boundary changes to first order. Following this first order line towards the origin, the jump height of the tilt azimuth across the line steadily increases until a jump of 30° is reached corresponding to the NN/NNN transition predicted by the model of Selinger and Nelson. Similar behavior is observed for the NN/I_2 transition, which is the mirror image of the NNN/I_1 transition reflected at the origin.

The phase behavior observed in the experiment may be understood in terms of this phase diagram as follows: at low temperature $h_{12} = 0$ is a good approximation. The Durbin model applies and on increasing d_2 starting from $d_2 < 0$ one moves in a clockwise direction on the unit circle in Figure 7 crossing the NN/I_1 boundary with a jump of tilt azimuth from 0 to 60° in the I_1 phase. Then the tilt azimuth gradually increases to 90° at $(d, h) = (0.993,\ 0.11)$ where the second order transition line to the NNN phase is crossed. This phase sequence is consistent with the phase sequence observed experimentally on increasing the surface pressure. It has been proven experimentally that at higher temperatures the distortion of the hexatic lattice is less pronounced and due to the possibility of a free rotation of the molecules around their molecular long axis may totally disappear. From this one concludes that d_2 should be much smaller at higher temperatures. On the other hand the first order transition from the NN to the NNN phase has been associated with a change in h_6. Therefore one concludes that also h_6 should be small in the vicinity of the *swiveling* transition. Assuming that h_{12} is negligible at low temperatures it may well be that at elevated temperatures it becomes comparable to d_2 and h_6. The path taken on increasing d_2 or decreasing h_6 at finite and positive h_{12} will lie within the unit circle of the phase diagram (see arrow in Fig. 7). Eventually the crossing of the NNN/I_1 boundary will occur at the first order line rather than at the second order boundary. The nearer to the origin this boundary is crossed the more the boundary adopts the character of a 60°/90°, *e.g.*, a NN/NNN transition and the narrower will be the I phase. The first order transition from 0° towards 60° occurring on changing the sign of d_2 will eventually be hard to detect as the distortion gets smaller. Hence the explanation of the behavior observed in experiment would be that the first and second order transition at low temperature is explained by the model of Durbin *et al.* ($h_{12} = 0$), but on increasing temperature h_{12} gets more and more comparable to h_6 and d_2 such that surface pressure region of the I phase narrows. The second order transition changes to first order with the I phase more and more adopting the character of a 60° NN phase and the I/L_2' transition more and more adopting the character of the *swiveling* transition. Correlated with this, the distortion of the hexatic lattice decreases and the 0°/60° transition joins the 60°/90° transition at $d_2 = 0$.

For $h_{12} = 0$ the behavior of the tilt azimuth angle within the I phase as a function of h_6 and d_2 may be solved analytically. One finds

$$(\varphi - \theta)_{min} = \pi \pm \sqrt{\frac{9h_6 - d_2}{12h_6}}\,. \tag{6}$$

This tilt azimuth shows typical mean field behavior near the I/L_2' transition, *e.g.*, it varies as the square root of the control parameter describing the distance to the transition. One may also solve for the spatial behavior of the tilt azimuth by including the elastic rigidity term in equation (4) and solving the Euler Lagrange equation. One obtains

$$\begin{aligned} x &= \frac{1}{2}\sqrt{\frac{K}{2h_6}} \int_{\pi}^{(\varphi-\theta)} \frac{1}{|\cos 2(\varphi-\theta) - \cos 2(\varphi-\theta)_{min}|} \\ &\quad \times \frac{d2(\varphi-\theta)}{\sqrt{-4(\cos 2(\varphi-\theta) + 2\cos 2(\varphi-\theta)_{min})}} \qquad (7) \\ &\approx \frac{1}{2}\sqrt{\frac{K}{2h_6}} \int_{\pi}^{(\varphi-\theta)} \frac{1}{|\cos 2(\varphi-\theta) - \cos 2(\varphi-\theta)_{min}|} \\ &\quad \times \frac{d2(\varphi-\theta)}{\sqrt{-12\cos 2(\varphi-\theta)_{min}}} \end{aligned}$$

with the result:

$$(\varphi - \theta)(x) = \arctan\left[\tan((\varphi - \theta)_{min}) \coth \frac{x}{\xi}\right], \qquad (8)$$

where

$$\xi = \sqrt{\frac{K}{-24h_6 \cos(2(\varphi - \theta)_{min})}} \frac{1}{8\sin(2(\varphi - \theta)_{min})}. \qquad (9)$$

This exactly describes the boundary of width ξ and height $2(\varphi - \theta)_{min}$ between two domains of opposite chirality as observed in the BAM measurements. According to equation (6) the disclination wall disappears as the L_2' (NN) phase is approached.

6 Conclusions

The low temperature intermediate phase in eicosanoic acid monolayers on an acidic subphase discovered by Durbin *et al.* has been confirmed using BAM. A characteristic finger print of the texture of the intermediate phase is the gradual occurrence of disclination walls on entering this phase from higher pressures. These disclination walls separate domains of opposite chirality but continuous hexatic order. The chiral order parameter, the relative tilt azimuth, measured with respect to the nearest neighbor distortion direction, follows a mean field behavior. A Landau free energy including distortion, hexatic and tilt azimuth order parameters is consistent with the phase behavior observed over a broad temperature range.

This work is dedicated to Prof. F. Schwabl in honor of his sixties birthday. The support of the German Science Foundation within the SFB 294: *Moleküle in Wechselwirkung mit Grenzflächen* is highly acknowledged.

References

1. M.K. Durbin, A. Malik, A.G. Richter, R. Ghaskadvi, T. Gog, P. Dutta, J. Chem. Phys. **106**, 8216 (1997).
2. J.V. Selinger, D.R. Nelson, Phys. Rev. Let. **61**, 416 (1988); Phys. Rev. A **39**, 3135 (1989).
3. I.R. Peterson, R.M. Kenn, A. Goudot, P. Fontaine, F. Rondelez, W.G. Bouwman, K. Kjaer, Phys. Rev. E **53**, 667 (1996).
4. X. Qiu, J. Ruiz-Garcia, C.M. Knobler, *Interface dynamics and growth*, edited by K.S. Liang, M.P. Anderson, R.F. Bruinsma, G. Scoles (Materials Research Society, Pittsburgh, 1992), p. 263.
5. C. Lautz, J. Kildea, Th.M. Fischer, J. Chem. Phys. **106**, 7448 (1997).
6. C. Lautz, Th.M. Fischer, J. Phys. Chem. **101**, 8790 (1997).
7. D. Hönig, D. Möbius, J. Phys. Chem. **95**, 4590 (1991).
8. D. Hönig, D. Möbius, Thin Solid Films **210-211**, 64 (1992).
9. D. Hönig, G.A. Overbeck, D. Möbius, Adv. Mater. **4**, 419 (1992).
10. G.A. Overbeck, D. Möbius, J. Phys. Chem. **97**, 7999 (1993).
11. S. Rivière, S. Hénon, J. Meunier, D.K. Schwarz, M.-W. Tsao, C.M. Knobler, J. Chem. Phys. **101**, 10045 (1994).
12. V.M. Kaganer, I.R. Peterson, R.M. Kenn, M.C. Shih, M. Durbin, P. Dutta, J. Chem. Phys. **102**, 9412 (1995).
13. C. Lautz, Th.M. Fischer, Jpn J. Appl. Phys. **36**, (1997).
14. M. Paudler, J. Ruths, H. Riegler, Langmuir **8**, 184 (1992).
15. Th.M. Fischer, R.F. Bruinsma, C.M. Knobler, Phys. Rev. E **50**, 413 (1994).